The effect of edge valency on the load resistance of single-layer reticulated cylindrical shells

Ranjith Kolakkattil[a,*], Konstantinos Daniel Tsavdaridis[b], Arul Jayachandran Sanjeevi[a]

[a]*Indian Institute of Technology Madras, Department of Civil Engineering, Chennai, 600036, Tamil Nadu, India*
[b]*City, University of London, Department of Civil Engineering, School of Mathematics, Computer Science and Engineering, London, EC1V 0HB, United Kingdom*

Abstract

The arrangement of members plays a crucial role in determining the resistance of reticulated cylindrical shells, in addition to rise-to-span ratio, cross-section of the members, rigidity of the joints, and support conditions. Although studies on the comparison of shell structures with different configurations are available, the effect of the member arrangement on the performance of reticulated shell structures based on the valency of elements was never investigated before. This paper investigates the effect of edge valency on the load resistance of shell structures by studying the behaviour of four cylindrical shell configurations with different edge valencies of vertices and faces. The limit load of the shell structures - with different rise-to-span ratios, length-to-span ratios, support conditions, load patterns, and different magnitudes of initial geometric imperfection – is calculated based on geometrical and material non-linear analyses. The results show that the increase in the edge valency of the vertices increases the overall resistance of single-layer reticulated cylindrical shells with rigid joints. In addition to edge valency, member orientation plays a prominent role in determining the overall resistance of single-layer reticulated shell structures with longitudinal edges supported. The data on edge valency help to rearrange the members within a structure so that the overall resistance is not compromised, while the designer aims for an economical solution.

Keywords: Reticulated cylindrical shells, parameterisation, valency, non-triangulation, limit load, global stability

*Corresponding Author
Email address: ranjithk@alumni.iitm.ac.in (Ranjith Kolakkattil)

1. Introduction

Barrel vault is a type of spatial structure used to cover large spaces without columns (Figure 1). They are developable surfaces with zero Gaussian curvature. The cylindrical shape provides more volume under the surface, and the resulting structure is more efficient than traditional grid systems. Triangulation is adopted for many structures due to the stability provided by the triangulated geometry. Single-layer triangulated cylindrical shells are robust and result in uniform stress distribution [1, 2]. They are constructed with members of equal length, and the resulting structure is lighter than other types of vaults [3]. The uniformity of member cross-section and equal length of members make these structures more popular and reliable due to the immense economic benefit. They are analysed and designed as structures with pin connection between the members. However, reticulated shells with non-triangulated faces should have rigid joints for adequate stability. The rigid joints make the structure more predictable, with lesser deflection and lesser variation in stress distribution. These reticulated shells can be adopted for structures with lower dimensions and lower load resistance requirements (Figure 1(b)).

Comparison of the performance of triangulated single-layer reticulated cylindrical shells with non-triangulated cylindrical shells is rare in the literature. In fact, most studies are conducted on triangulated cylindrical shells because of their superior performance and popularity. The experimental test on single-layer barrel vaults found that bracing influences the stability and overall resistance of the structure [3]. The three-way arrangement of the members results in uniform stress distribution and smaller deflections in the structure, especially under non-uniform load distribution [3]. The presence of rigid joints greatly influences the stress distribution and the deflection in reticulated shells. Parke obtained the most economical rise-to-width (rise-to-span) ratio as 0.17 from the comparative analysis of the strength-to-weight ratio and the stiffness of three reticulated cylindrical configurations [4]. The shell with a rise-to-span ratio of 0.17 was found to be the lightest and experienced the least deflection, the maximum axial force, and the minimum bending moment in the cases of symmetric and asymmetric load. Gioncu explained the different parameters affecting the stability of triangulated barrel vaults and instability modes in spatial structures, such as member, node, line, and overall instability [5]. Many studies have been conducted on single-layer reticulated domes, which are applicable to cylindrical shells to a great extent. Abedi conducted experimental studies on reticulated domes, including the dynamic behaviour of nodal snap-through buckling by inducing initial velocities at the node [6]. Lenza studied the dynamic effect of the snap-through buckling on doubly curved shells [7]. Kato et al. investigated the impact of the slenderness of the members on the global stability of single-layer domes [8]. Yamada et al. studied the imperfection sensitivities in single-layer lattice domes [9]. Lopez et al. conducted the numerical and experimental investigation on a single-layer lattice dome with semi-rigid joints [10]. Fan et al. studied

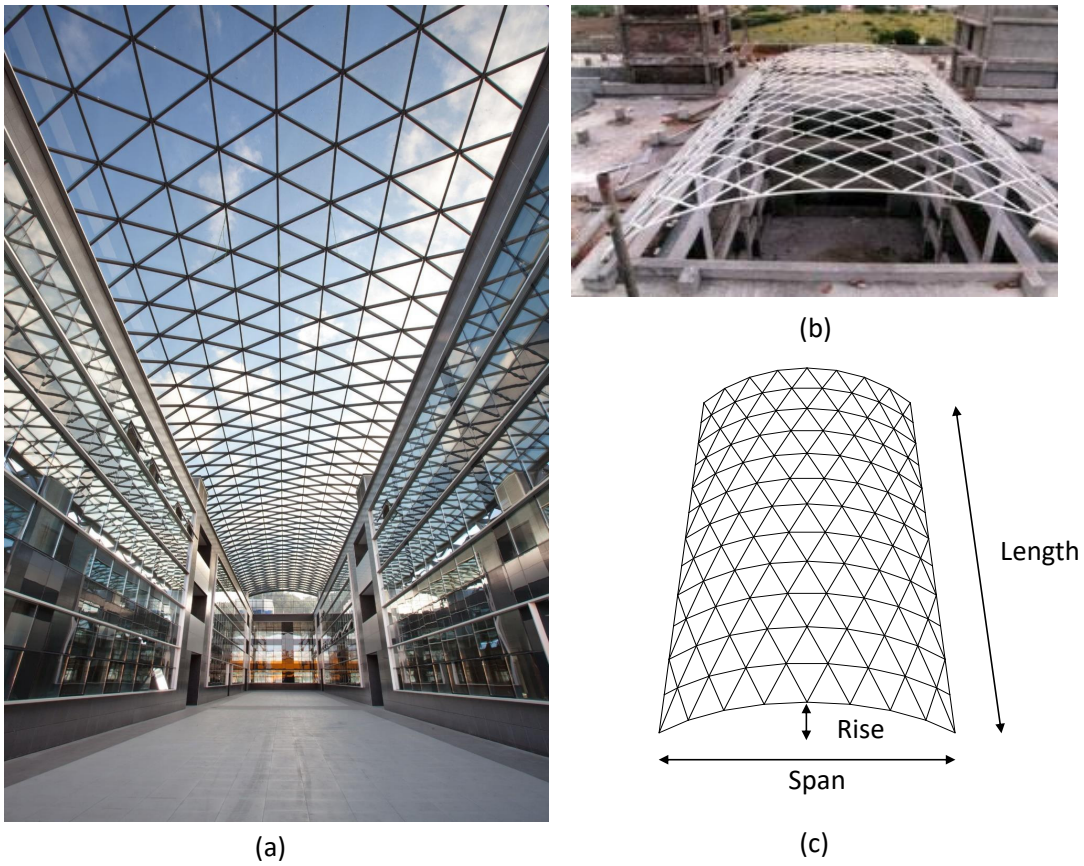

Figure 1: Examples of single-layer reticulated cylindrical shells: (a) Merineda City Shopping Mall, A Coruña (reproduced with permission from Lanik, Spain) (b) BT Savani Hospital, Rajkot (reproduced with permission from Lakhlani Associates, India) (c) Dimensions of a single-layer reticulated cylindrical shell

the elasto-plastic stability of single-layer reticulated dome structures [11]. Yan et al. studied the 'coupled instability behaviour' in single-layer reticulated dome structures, where the interaction between member buckling and overall buckling of the structure was investigated [12]. Reticulated structures are very sensitive to imperfections due to the spatial arrangement of the members. Several studies have incorporated the effect of imperfection in reticulated shell structures. Although it is difficult to introduce actual imperfections into the structures, there are methods available to model shell structures, which provide the least favourable position of members and nodes [13]. The effect of the initial curvature of the members on the elasto-plastic stability and the member buckling was explored by Fan et al. [14]. Consideration of imperfections will result in a reduction of load resistance of the structures. Therefore, imperfection analysis is necessary while analysing any shell structure. In fact, structural imperfection sensitivity can be included in the shape optimisation of structures such that the resulting geometry has a high buckling load [15].

Limited studies are available on the performance comparison of cylindrical shells with different configurations. Parke investigated the optimum member arrangement among the triangulated configurations [4]. Later, the effect of member arrangement was studied in detail by considering the stiffness-weight ratio, strength-weight ratio, stress distribution, and redundancy of 13 single-layer cylindrical shells [16, 17]. The significance of transverse members, longitudinal members, and bracing members was identified in the study (Figure 2). The author also noted that the absence of bracing members (i.e., the absence of triangulation) resulted in a lack of integrity between the elements, and the stability of those reticulated shell structures depended primarily on the rigidity of the joints. A similar study considering the imperfection in the shell structures concluded that the lack of bracing members would increase the sensitivity towards imperfections due to the inability to transfer forces between the 'segments' [18]. Later, an extensive parametric study of triangulated vaults showed the influence of asymmetric load, support condition, material yield stress, and geometry of the collapse mechanism on the load-carrying capacity [19]. These studies demonstrate that triangulated structures are always stable and economical in comparison to non-triangulated shell structures.

As the fundamental difference among shell configurations is their connectivity between members, investigation of the relationship between the connectivity of the members and the load capacity of the shell structures is of great interest. The connectivity between the members can be redefined based on the parameter "Valency", one of the 'parameters of structures' defined by Loeb [20]. Parameters such as valency are helpful in creating different non-triangulated dome configurations [21]. Load capacity, material use, redundancy, stress distribution, and aesthetic appearance will vary among these reticulated shell structures. Although comparisons of different cylindrical shell configurations have been made earlier, the effect of valency on the global stability of reticulated shells is rarely mentioned

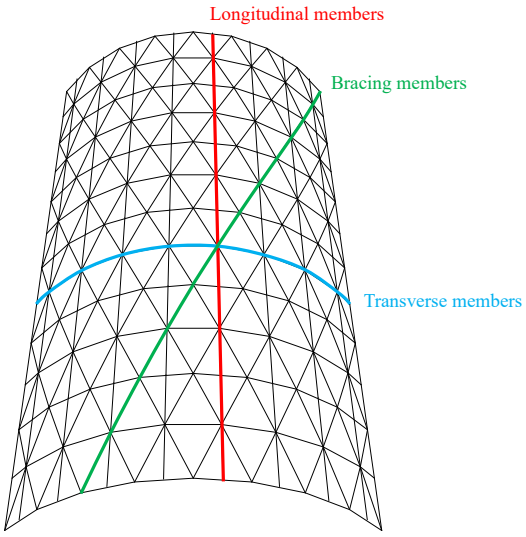

Figure 2: Members defined as per their orientation in a cylindrical shell structure

in the literature. Hence, an attempt has been made in this paper to study the influence of edge valency of vertices on the overall resistance of single-layer reticulated cylindrical shells. Different cylindrical shells with varying edge valency are subjected to Geometrical and Material Nonlinear Analysis (GMNA) [22]. The performance of these cylindrical shells is compared to the average edge valency of vertices and faces. The study identifies the importance of considering edge valency in optimising the performance of rigid-jointed structures.

2. Configuration based on the valency of elements

Any reticulated structure can be defined as a combination of vertices, edges, faces, and cells (Figure 3). Two vertices help to form an edge, three or more edges combine to create a face, and four or more faces combine to form a cell. As a result, these elements are related to each other. Three parameters can be introduced to define the relationship between the elements. Loeb defined them as the 'parameters of structures': dimensionality, valency, and extent [20].

2.1. Parameters in a structure

The first parameter, 'dimensionality,' is the degree of freedom of an element. For example, the dimensionality of a vertex is zero since it has zero degrees of freedom. Similarly, the dimensionality of an edge, face, and cell is one, two, and three, respectively. A

structure can be redefined as the combination of elements with dimensionalities of zero, one, two, and three. Similar to the way elements with different dimensionalities are related to each other, the total number of elements with different dimensionalities are related to each other within a structure, based on the equation named 'Euler-Schlaefli relation' (Equation 1).

$$\sum_{i=0}^{j}(-1)^i N_i = 1 + (-1)^i \tag{1}$$

N_i denotes the number of elements with dimensionality i. For example, N_0 is the number of vertices in a structure. j denotes the number of dimensions considered for a structure (e.g., $j = 2$ for a two-dimensional structure and $j = 3$ for a three-dimensional structure). For two-dimensional structures, Equation 1 is simplified to Equation 2, and for three-dimensional structures, Equation 1 is simplified to Equation 3. These equations ensure that the configurations are in 'closed-form', i.e., open-ended edges or faces are not present in the configurations. Therefore, the equations ensure that the elements of a configuration are restricted.

$$N_0 - N_1 + N_2 = 2 \tag{2}$$

$$N_0 - N_1 + N_2 - N_3 = 0 \tag{3}$$

The second parameter, 'Valency,' is the sum of elements of a certain dimensionality that are connected to an element of a different dimensionality. For example, the edge valency of a vertex in a cube is three because it is directly connected to three edges (Figure 3). Similarly, the vertex valency and the edge valency of any face in the cube are four, and the vertex valency of the cell is eight. Different combinations of elements result in different valencies, as there are four elements with different dimensionality available in a three-dimensional structure (Table 1). The vertex valency of an edge and the cell valency of a face are always two ($E_0 = F_3 = 2$) for every configuration. Similarly, the face valency of an edge and the cell valency of an edge are always identical ($E_2 = E_3$), and the vertex valency of a face and the edge valency of a face are always identical ($F_0 = F_1$). As a result, the total number of valencies in a three-dimensional structure will be reduced to eight. Only six of the eight valencies are independent, and the remaining two can be found from the relations obtained from the Euler-Schlaefli equation (Equation 4 and Equation 5).

$$V_1 - V_2 + V_3 = 2 \tag{4}$$

$$C_0 - C_1 + C_2 = 2 \tag{5}$$

The third parameter – 'extent' – is the measurable quantity within a structure, such as

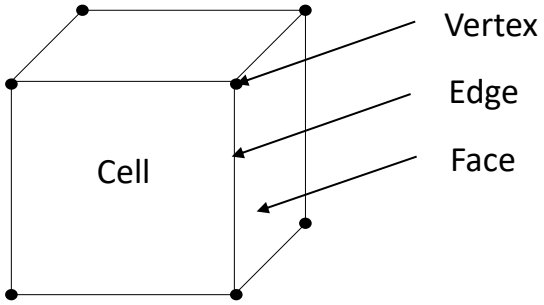

Figure 3: A cube explaining the elements and valencies in a reticulated structure

Table 1: Different valencies in a configuration

Element	Vertex Valency	Edge Valency	Face Valency	Cell Valency
Vertex	-	V_1	V_2	V_3
Edge	2	-	E_2	E_3
Face	F_0	F_1	-	2
Cell	C_0	C_1	C_2	-

length, area, and volume. The third parameter is critical for a reticulated structure since it is directly related to the cost of the structure.

2.2. Interdependency of the valencies

The valencies in a structure are related to each other, and elements – such as edges and nodes – can be found from the restrictions derived from the interdependence of the valencies.

The number of edges in a structure is obtained by summing the edge valency of all the vertices in the structure. Let N_0^r be the number of vertices whose edge valency is r. Then summing the edge valency of all the vertices will result in:

$$2N_0^2 + 3N_0^3 + 4N_0^4 + ... = \sum_{r=2}^{n} rN_0^r \tag{6}$$

The sum of edge valency of all the vertices equals the sum of vertex valency of all the edges in a structure.

$$\sum_{r=2}^{n} rN_0^r = \sum_{s=2}^{n} sN_1^s \tag{7}$$

The vertex valency of an edge is always two. As a result, $s = 2$ and $sN_1^s = N_1$. Therefore, Equation 7 is modified to:

$$\sum_{r=2}^{n} rN_0^r - 2N_1 = 0 \tag{8}$$

Equation 8 helps to find the number of edges in a structure from the edge valency of all the vertices. For example, a basic unit such as a triangle has three edges ($N_1 = 3$), and the summation of the edge valency of the vertices gives twice the number of the edges (Equation 9).

$$\sum_{r=2}^{n} rN_0^r = 2N_0^2 = 6 \tag{9}$$

The total number of vertices in a structure is given by:

$$N_0 = \sum_{r=2}^{n} N_0^r \tag{10}$$

Valency can change from position to position in structures like reticulated shells. Therefore, the average edge valency of vertices is defined as follows:

$$\bar{v_1} = \sum_{r=2}^{n} \frac{rN_0^r}{N_0} \tag{11}$$

From Equations 8 and 11, the relation between the number of vertices, edges, and the average edge valency of vertices is derived as follows:

$$\bar{v_1}N_0 - 2N_1 = 0 \tag{12}$$

The sum of face valency of all edges and the sum of edge valency of all faces in a structure are equal. i.e.,

$$\sum_{t=2}^{n} tN_1^t = \sum_{u=3}^{n} uN_2^u \tag{13}$$

Similar to Equation 11, the average value of face valency of edges and edge valency of faces are computed as follows:

$$\bar{e_2} = \sum_{t=2}^{n} \frac{tN_1^t}{N_1} \tag{14}$$

$$\bar{f_1} = \sum_{u=3}^{n} \frac{uN_2^u}{N_2} \tag{15}$$

From equations 13, 14, and 15, the relation between the number of edges, the number of faces, the average edge valency of faces, and the average face valency of edges in a structure is derived as follows:

$$\bar{e_2}N_1 - \bar{f_1}N_2 = 0 \tag{16}$$

Similarly, the relation between cell valency of edges and edge valency of cells is:

$$\sum_{w=3}^{n} wN_1^w = \sum_{x=6}^{n} xN_3^x \tag{17}$$

The cell valency of the edges and the face valency of the edges are always equal ($w = t$). Therefore, Equation 17 is modified to:

$$\sum_{t=3}^{n} tN_1^t = \sum_{x=6}^{n} xN_3^x \tag{18}$$

The average edge valency of cells is defined as follows:

$$\bar{c_1} = \sum_{x=6}^{n} \frac{xN_3^x}{N_3} \tag{19}$$

From Equations 14, 18, and 19, the relation between the number of edges, the number of cells, the average face valency of edges, and the average edge valency of cells is derived as follows:

$$\bar{e_2}N_1 - \bar{c_1}N_3 = 0 \tag{20}$$

Similar expressions can be obtained for vertex-face valency relation:

$$\sum_{y=2}^{n} yN_0^y = \sum_{z=3}^{n} zN_2^z \tag{21}$$

The vertex valency of faces is equal to the edge valency of faces ($z = u$). Therefore, Equation 21 is modified to:

$$\sum_{y=2}^{n} yN_0^y = \sum_{u=3}^{n} uN_2^u \tag{22}$$

The average vertex valency of face and the average face valency of vertex are:

$$\bar{f_0} = \sum_{u=3}^{n} \frac{uN_2^u}{N_2} \tag{23}$$

$$\bar{v_2} = \sum_{y=2}^{n} \frac{yN_0^y}{N_0} \tag{24}$$

From equations 22, 23, and 24, the relation between the number of vertices, the number of faces, the average face valency of vertices, and the average vertex valency of faces is derived:

$$\bar{v_2}N_0 - \bar{f_0}N_2 = 0 \tag{25}$$

The sum of vertex valency of all cells is equal to the sum of cell valency of all vertices in a structure (Equation 26).

$$\sum_{a=2}^{n} aN_0^a = \sum_{b=6}^{n} bN_3^b \tag{26}$$

The average vertex valency of cells and the average cell valency of vertices are:

$$\bar{c_0} = \sum_{b=6}^{n} \frac{bN_3^b}{N_3} \tag{27}$$

$$\bar{v_3} = \sum_{a=2}^{n} \frac{aN_0^a}{N_0} \tag{28}$$

From equations 26, 27, and 28, the relation between the number of vertices, the number of cells, the average cell valency of vertices, and the average vertex valency of cells is derived as follows:

$$\bar{v_3}N_0 - \bar{c_0}N_3 = 0 \tag{29}$$

The sum of face valency of all cells is equal to the sum of cell valency of all faces in a structure (Equation 30).

$$\sum_{d=2}^{n} dN_2^d = \sum_{g=4}^{n} gN_3^g \tag{30}$$

The cell valency of a face is always two ($d = 2$). Hence, Equation 30 is modified to:

$$\sum_{g=4}^{n} gN_3^g - 2N_2 = 0 \tag{31}$$

The average face valency of cells is given by:

$$\bar{c_2} = \sum_{g=4}^{n} \frac{gN_3^g}{N_3} \tag{32}$$

From Equations 31 and 32, the relation between the number of faces, the number of cells, and the average face valency of cells is obtained as:

$$\bar{c_2}N_3 - 2N_2 = 0 \tag{33}$$

From Equations 16, 20, and 25:

$$\bar{e_2}N_1 = \bar{f_1}N_2 = \bar{c_1}N_3 = \bar{v_2}N_0 \tag{34}$$

Expressing N_1, N_2, and N_3 in terms of N_0 and substituting in Equation 3 will result in:

$$\frac{1}{\bar{v_2}} - \frac{1}{\bar{e_2}} + \frac{1}{\bar{f_1}} - \frac{1}{\bar{c_1}} = 0 \tag{35}$$

Equation 35 connects the average vertex valency of face, average edge valency of face, average face valency of edge, and average cell valency of edge.

From equations 12,16, and 25:

$$\bar{v_1}\bar{e_2} - 2\bar{v_2} = 0 \tag{36}$$

If reticulated cylindrical shell configurations are considered as a two-dimensional net, the face valency of all the edges will be two ($\bar{e_2} = 2$). Hence, Equation 36 is modified to:

$$\bar{v_1} - \bar{v_2} = 0 \tag{37}$$

As a result, Equation 4 will result in $\bar{v_3} = 2$. The two-dimensional configurations divide the space into two ($N_3 = 2$). Substituting these values in Equation 20 will lead to:

$$N_1 - \bar{c}_1 = 0 \tag{38}$$

The results of Equations 36, 37, and 38 will modify Equation 35 as follows:

$$\frac{1}{\bar{v}_1} + \frac{1}{\bar{f}_1} - \frac{1}{N_1} - \frac{1}{2} = 0 \tag{39}$$

Equation 39 is valid for any configuration in two-dimension [20]. Although the single-layer lattice cylindrical shells are three-dimensional in nature, they can be considered as a two-dimensional net. As the number of edges is constant for a selected cylindrical shell, the values of average edge valency of vertices and average edge valency of faces are inversely proportional to each other. The effect of these factors on the overall resistance of the single-layer reticulated shells is investigated in this paper.

2.3. Nomenclature based on the edge valency

The three parameters are helpful in creating different single-layer reticulated shell configurations (Figure 4). As the parameters vary for each configuration, a nomenclature can be generated based on the selected parameters, such as valency, so that the nomenclature itself can describe the important properties of the configuration [21].

The edge valence of the vertices and the edge valence of the faces are used when creating the nomenclature for single-layer reticulated shell configurations. Regularly used shell structures, such as triangulated shell structures, have identical edge valency of vertices and faces on the inner surface (Figure 5). The nomenclature for these configurations starts with the notation 'V' to identify that the edge valency of vertices is used during the generation of the nomenclature. The edge valency of vertices for a cell is arranged in the clockwise direction to arrive at the required nomenclature. For example, the nomenclature based on the edge valency of vertices for the triangulated configuration is V.6.6.6 or V.6^3 (Figure 5). Nomenclature is provided for the selected configurations similarly (Figure 6). A nomenclature provided for a single-layer shell configuration provides a good deal of information about a structure. As stated earlier, 'V' indicates that the edge valency of vertices in a face is used while generating the nomenclature. The number of edge valencies in the nomenclature (three in the example given in Figure 5) provides the edge valency (and the vertex valency) of each face in the structure. Each digit (six in the example) provides the edge valency of vertex for each vertex in a face. The edge valency of vertex gives the angle between the members in the plane of the reticulated shell. Here, the digit 'six' in the nomenclature implies that the 'in-plane angle' between the members is 60 degrees (Figure 7). Therefore, the nomenclature can capture the arrangement of members and the parameters in a configuration, such as the connections and angle between members. Additional parameters such as rise (R), span (S), length (L), and member cross-sections

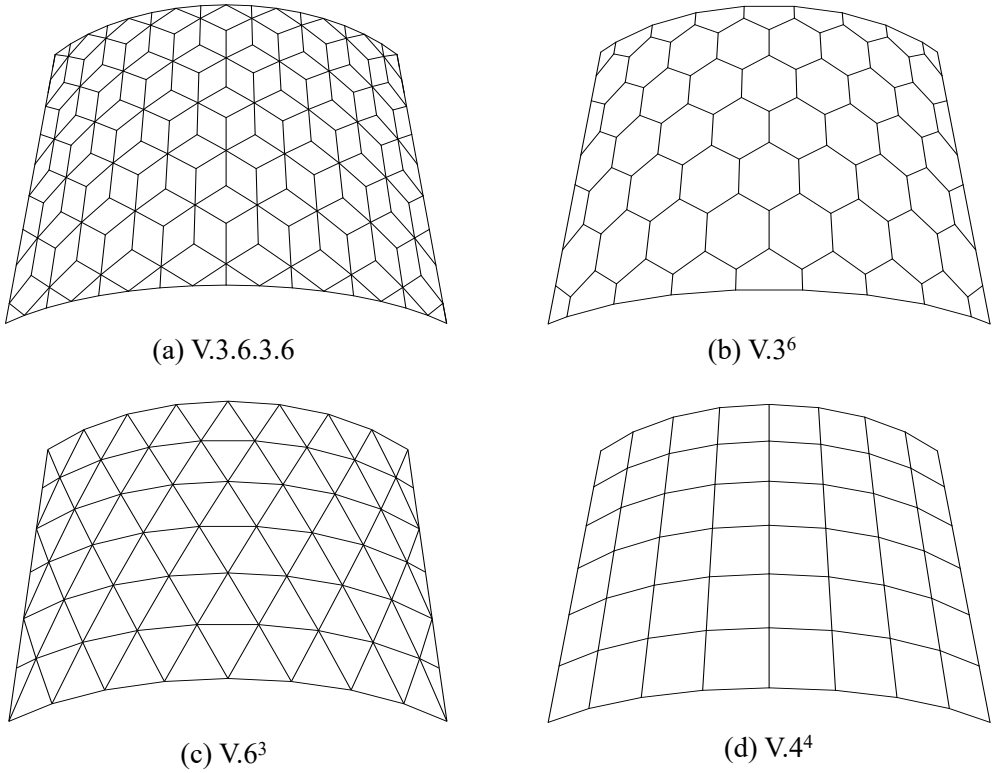

(a) V.3.6.3.6 (b) V.3^6

(c) V.6^3 (d) V.4^4

Figure 4: Types of parameterised reticulated cylindrical shells used in the study. Nomenclature [21] based on parameterisation principles is provided along with each cylindrical shell

can be included in the nomenclature to obtain the complete details of a reticulated shell configuration.

2.4. Effect of edge valency

The connection rigidity of the single-layer reticulated shell configurations with edge valency of face more than three should be maximum for obtaining a stable structure. Therefore, rigid-jointed structures are used for the present study, even if triangulation is present in the configuration. The edge valency should play a crucial role in the global and local stability of every shell configuration. The effect of the defined parameters – edge valency of vertices and edge valency of faces – are rarely compared in the earlier literature. Even though a comparison of the performance of different shell configurations was conducted earlier [4, 16, 17, 18], the effect of valency was never introduced. To evaluate the effect of the parameter – edge valency – on the global stability of single-layer reticulated cylindrical shell configurations, different configurations with different edge valencies

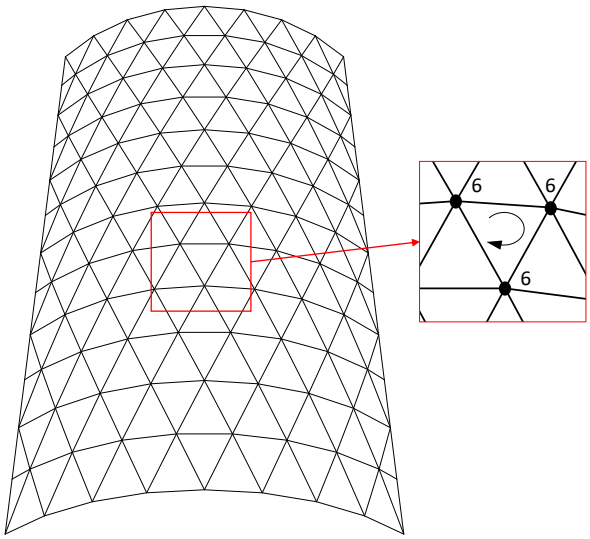

Figure 5: V.6^3: The nomenclature assigned to the configuration by arranging the edge valency of vertices in the clockwise direction

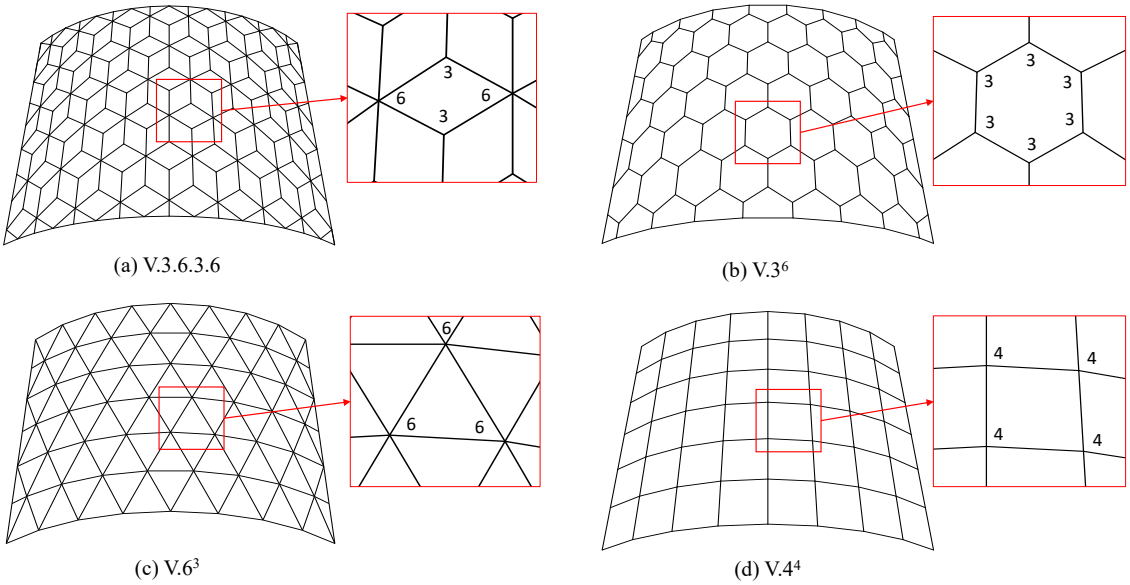

(a) V.3.6.3.6

(b) V.3^6

(c) V.6^3

(d) V.4^4

Figure 6: Nomenclature assigned to the four reticulated cylindrical shell configurations

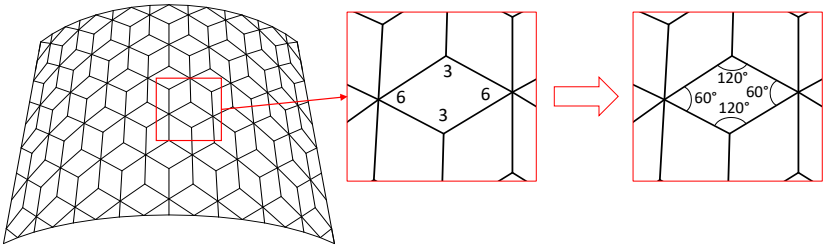

Figure 7: Edge valency provides the information on the in-plane angle between the members. In-plane angle between the members is 120°, 90° or 60° if the edge valency is 3, 4 or 6, respectively

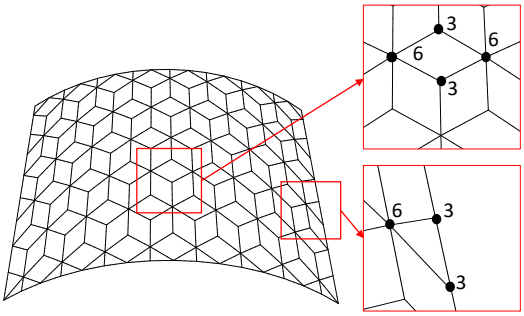

Figure 8: Difference in the edge valency of vertices at the edge region compared to that at the interior region of the shell configuration

of vertices and different edge valencies of faces (Figure 4) are selected and subjected to Geometrical and Material Nonlinear Analysis.

The edge valency of the vertices and faces can be different at the edge of the shell structure from that at the interior region for cylindrical shell structures. For example, the edge valency of vertices and faces are different for the configuration V.3.6.3.6 at the interior region from the support region (Figure 8). Hence, average edge valency of vertices ($\bar{v}_1$) and faces ($\bar{f}_1$) are calculated for the selected single-layer cylindrical shells to compare the overall resistance (Equation 11 and Equation 15). Although the average edge valency of vertices and faces varies from the actual edge valency of the shell configurations (that is, the edge valency of vertices and faces in the interior region), the difference will reduce once the span of the shell structure increases (Table 2).

3. Comparison of the overall resistance of the shell configurations with respect to edge valency

The overall resistance of the selected shell configurations was calculated by Geometrical and Material Nonlinear Analysis and compared with their average edge valency of

Table 2: Average edge valency of vertices and faces for the shell configurations with varying length-to-span ratios

Configuration	L1		L2	
	$\bar{v_1}$	$\bar{f_1}$	$\bar{v_1}$	$\bar{f_1}$
V.3.6.3.6	3.906	3.850	3.907	3.858
$V.3^6$	2.967	5.5	2.982	5.622
$V.6^3$	5.061	3.0	5.3	3.0
$V.4^4$	3.492	4.0	3.624	4.0

vertices and faces. The span-to-rise ratio, length-to-span ratio, support condition, and load distribution pattern were varied in the analysis to examine the applicability of the results in the selected shell configurations (Figure 4).

3.1. Finite Element Modelling

The configuration data for nodes and members of the cylindrical reticulated shells were created using Formex Algebra [23]. The shell structures were modelled by the finite element package, Abaqus [24], using Timoshenko beam element 'B31' (two-node linear beam) with each member divided into four beam elements. Circular hollow sections with an outer diameter of 48.3 mm and thickness of 3.2 mm were adopted for all the members [25]. The structural steel with yield strength of 250 MPa and Young's Modulus of 200 GPa with elastic-perfectly plastic constitutive relation was used for the finite element modelling (Figure 9). The member cross-section was arrived at based on IS 800 – Indian code of practice for general construction in steel [26]. The slenderness ratio of the members was limited to 110, and the buckling of the individual members was avoided. The overall resistance of the shell structures was calculated by finding the limit load from the load-deflection response (Figure 10).

3.2. Parametric Analysis

The parametric analysis adopted different span-to-rise ratios, two length-to-span ratios, two support conditions, and two load cases. The span of the shell configurations was fixed at 10 metres. A lower span was adopted, since cylindrical shells with non-triangulation and rigid joints are usually utilised for structures with a lower span. The span-to-rise ratio of the shell structures varied from 1/10 to 1/2 (denoted as R10 to R2). Length-to-span ratios of 1 and 2 were considered for all the configurations (denoted as L1 and L2). The supported conditions adopted were: (1) LES – Longitudinal Edges Supported, and (2) AES – All Edges Supported (Figure 11). Two gravity load patterns were considered in

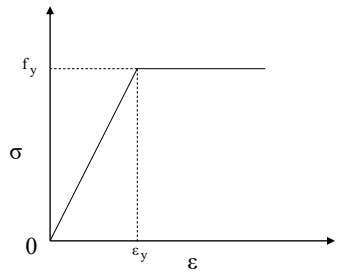

Figure 9: Elastic—perfectly plastic constitutive relation adopted for the shell structures (σ = Engineering stress, ϵ = Engineering strain, f_y = Yield stress, and ϵ_y = Yield strain)

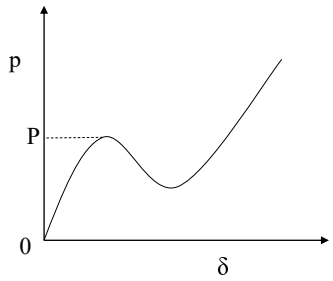

Figure 10: Limit load calculated for comparing the performance of cylindrical shell structures (p = Load applied per unit area, δ = Vertical deflection of the node, and P = Limit load)

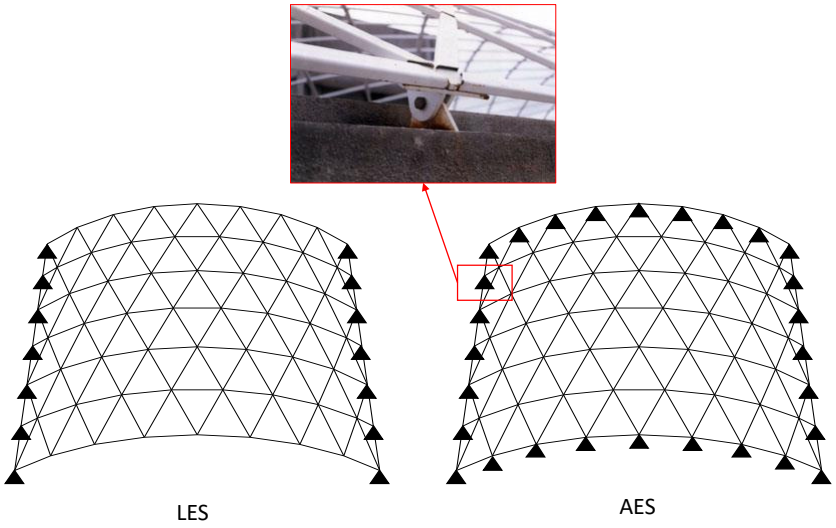

Figure 11: Different types of support conditions adopted in the study : (a) LES: Longitudinal edges are pin supported (b) AES: All the edges (both longitudinal edges and the transverse edges) are pin-supported. The sample picture of pin-connection is reproduced with permission from Lakhlani Associates, India

the investigation: (1) FL – Full-span gravity load covering the entire surface of the shell structure, and (2) HL – Half-span gravity load covering half the surface from the apex of the shell structure (Figure 12). Asymmetric load distribution analysis is critical for regions with heavy snow fall, and it had caused the failure of reticulated structures in the past [27]. Therefore, the effect of half-span gravity loading was considered in the analysis in addition to full-span gravity load. The limit load of the structure is determined by varying the mentioned parameters, and the results are examined with respect to the edge valency of the corresponding shell configuration.

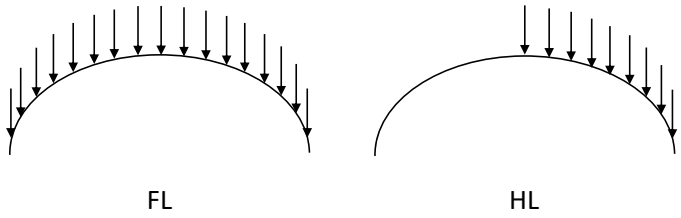

Figure 12: Load patterns considered in the study : (a) FL: Full-span gravity load (b) HL: Half-span gravity load

The primary objective of the study was to find the influence of edge valency on the overall resistance of the selected configurations. Many parameters, such as member length and connection numbers, must be identical in order to have a fair comparison of the performance of the four configurations. However, it was difficult to keep these parameters identical for the given configurations due to the interdependence of different elements (Table 3). It is quite evident from the table that keeping one element identical across all four configurations will result in large variations in other elements. Hence, configurations were tried to modify with the total weight ('extent' corresponding to the element 'length') of the elements being identical, which resulted in a large variation of the length among individual members. The chance of buckling of the members increased in configurations such as $V.6^3$ due to this large variation in length. This problem was avoided by keeping the length of individual members within a range such that the slenderness ratio of the members lies within a defined range. A new parameter (λ) was introduced to reduce the effect of variation on the total weight of the cylindrical shell structures while comparing their limit load (Equation 40). Here,'P' is the limit load and 'W' is the total weight of the structure. The weight of the connections was not considered while calculating the total weight of the structure. The members were welded to each other, and the contribution of the weight of the welding material was insignificant compared to the total weight of the shell structure.

Table 3: Variation in number of elements in cylindrical shell configurations

Configuration	N_0	N_1	N_2
V.3.6.3.6	170	332	147
$V.3^6$	122	181	60
$V.6^3$	66	167	102
$V.4^4$	63	110	48

$$\lambda = \frac{P}{W} \tag{40}$$

3.2.1. Variation of limit load with the rise-to-span ratios

The comparison of the limit load (P) and the parameter 'λ' with the change in the rise-to-span ratios when the shell structure was subjected to uniform gravity load is provided in Figure 13. The same comparison is provided separately for $V.6^3$ configuration with AES support condition (Figure 14), as there was a considerable variation in the values from those of other shell structures. It is evident from the above pair of graphs that converting the limit load to λ to compare the performance of the four configurations does

not alter their behaviour across different rise-to-span ratios. For example, the rise-to-span ratio corresponding to the maximum load resistance for the configuration V.6^3, with longitudinal edges supported, is between 0.167 and 0.2. The rise-to-span ratio corresponding to the maximum λ value lies on the same interval. The optimum rise-to-span ratio obtained by Parke was 0.17 for a similar shell structure with translational restraint provided at the longitudinal edges [4]. Hence, λ is used in the subsequent sections to compare the performance of all the configurations considered.

Different configurations have different rise-to-span ratios corresponding to maximum load capacity. The rise-to-span ratio corresponding to the maximum value of λ when longitudinal edges are supported is 0.25 for the configurations V.3.6.3.6 and V.3^6; the rise-to-span ratio corresponding to the maximum value of λ is between 0.167 and 0.2 for the configuration V.6^3, and 0.167 for V.4^4. For configurations with all the edges supported, the maximum value of λ was observed for shell structures with a rise-to-span ratio of 0.33 in all configurations.

Configurations with LES support condition have a lower rise-to-span ratio corresponding to maximum load capacity than those with AES support condition. For example, the rise-to-span ratio corresponding to the highest load capacity for the configuration V.3.6.3.6 with LES support condition is 0.25. However, the rise-to-span ratio for the maximum load capacity for the same configuration with all the edges supported is 0.33. A similar observation was made for all four shell structures. Additional supports at the curved edges provide additional load paths that cause an increase in load capacity with the rise of the shell. However, as the rise becomes very high, the members become more slender, and hence the load capacity is reduced. The structure cannot withstand a higher magnitude of load for shell configurations with only longitudinal edges supported because it has limited load paths compared to shell structures with all edges supported. As a result, they are deflected with a higher magnitude of deflection when subjected to a lower magnitude of external load (Figure 15). The effect of variation in the configuration (change in edge valency) is greater in shell structures with all edges supported compared to shell structures with only longitudinal edges supported. All configurations with LES support have similar buckling mode shapes when subjected to uniform gravity load (Figure 16). However, the first buckling mode shape of the V.6^3 was different from other configurations when all edges were pin-supported (Figure 17). This observation signifies the impact of variation in the edge valency on the performance of reticulated shell structures with all edges supported. However, non-linear analysis needs to be conducted to validate the result, which is performed in the next section.

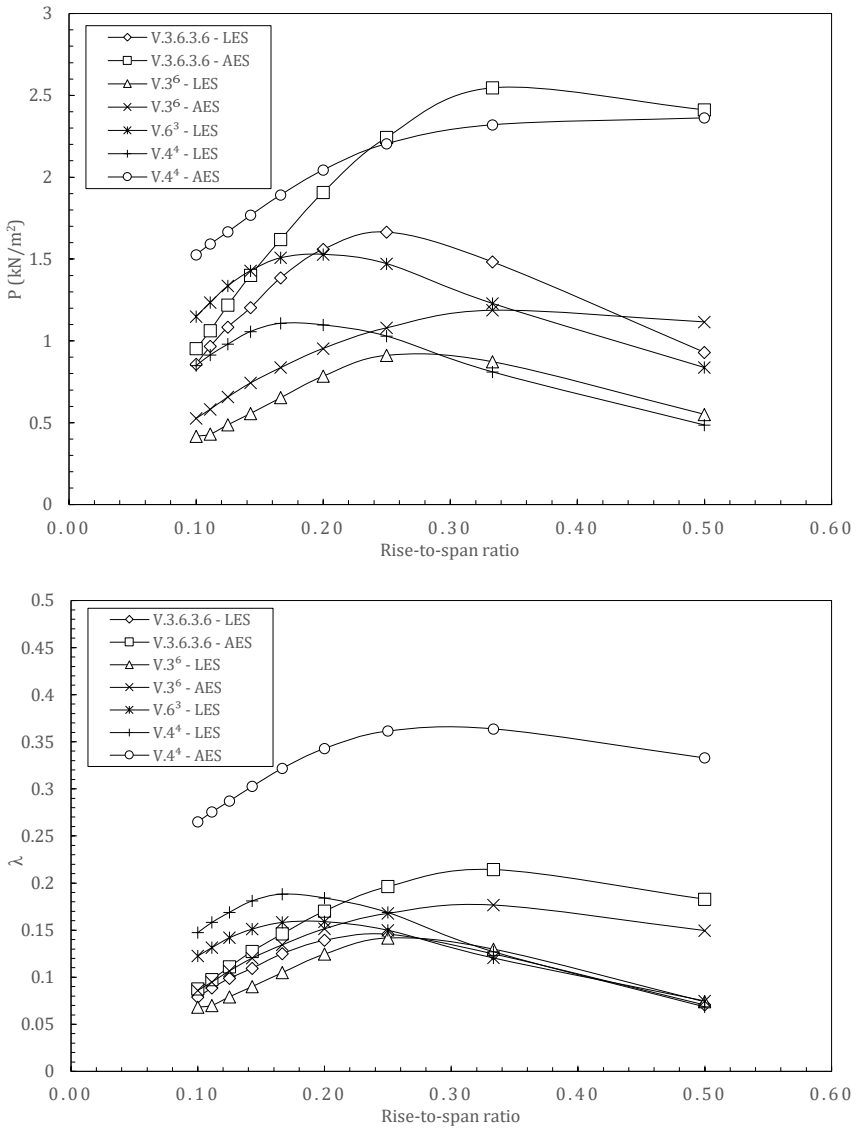

Figure 13: Variation of the limit load (P) and λ of cylindrical shell configurations with different rise-to-span ratios when shell structures were subjected to uniform gravity load

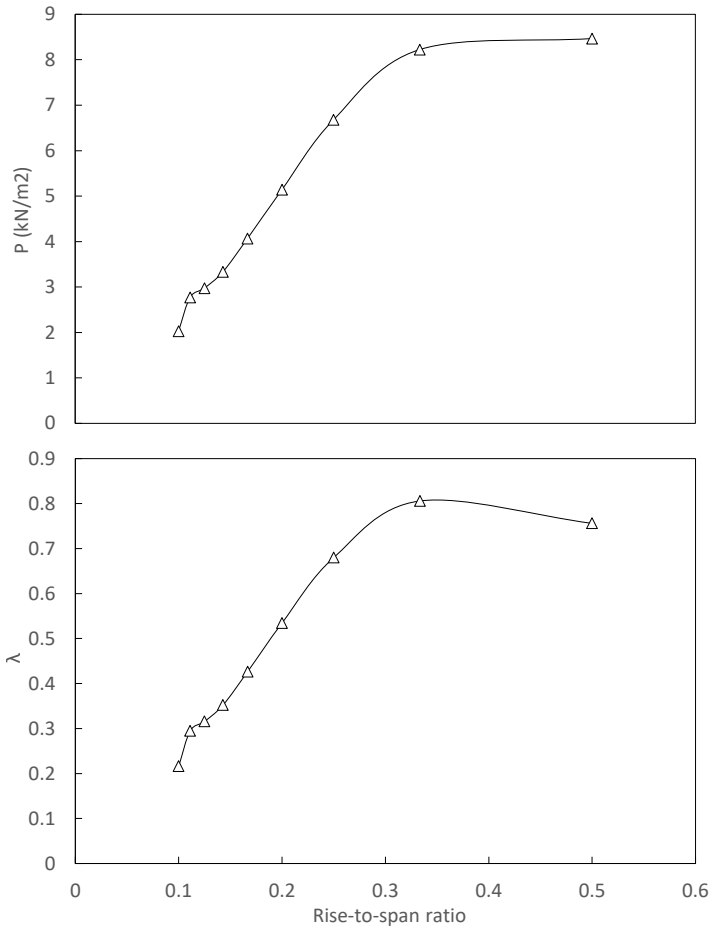

Figure 14: Variation of limit load (P) and λ of V.6[3] configuration with different rise-to-span ratios (AES support condition) when shell structure was subjected to uniform gravity load

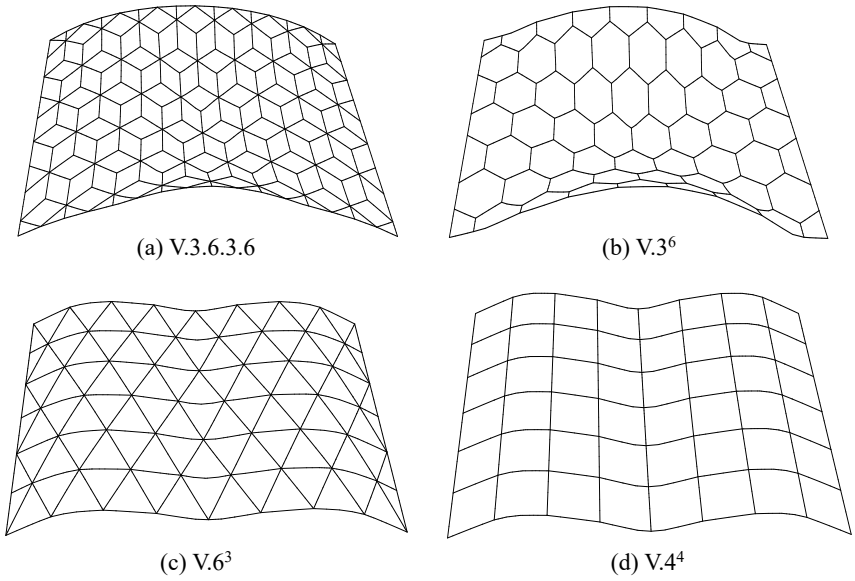

(a) V.3.6.3.6 (b) V.3^6

(c) V.6^3 (d) V.4^4

Figure 15: Deflected profile for the configurations with LES support condition when subjected to uniform gravity load

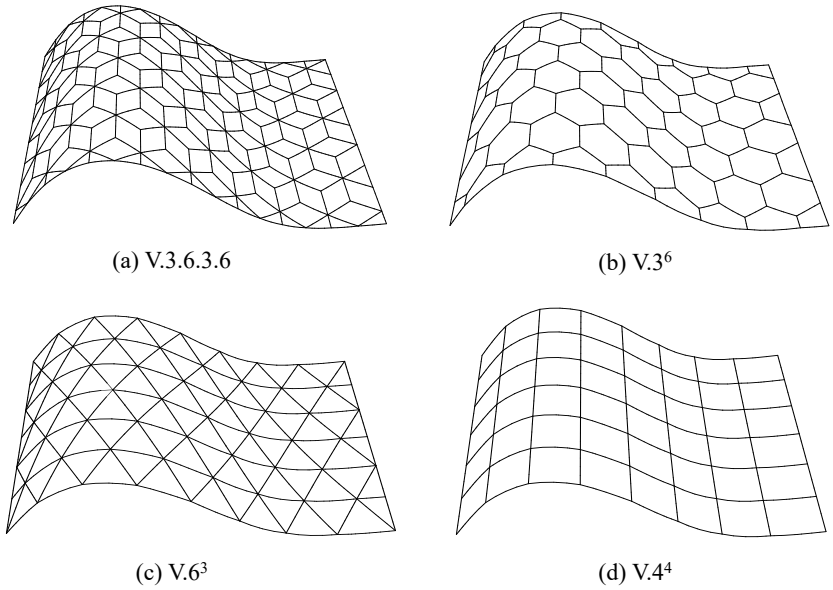

(a) V.3.6.3.6 (b) V.3^6

(c) V.6^3 (d) V.4^4

Figure 16: First buckling mode for the shell configurations with LES support condition when subjected to uniform gravity load

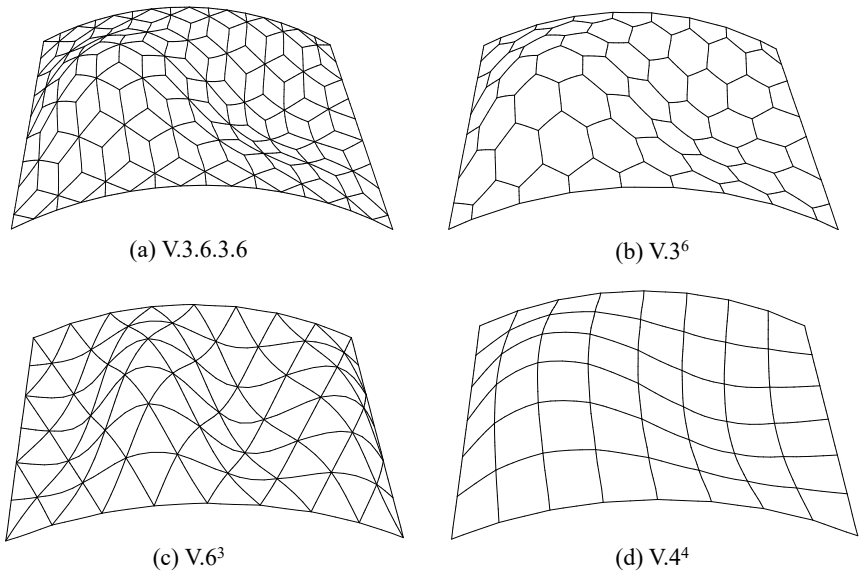

(a) V.3.6.3.6 (b) V.3^6

(c) V.6^3 (d) V.4^4

Figure 17: First buckling mode for the shell configurations with AES support condition when subjected to uniform gravity load

3.2.2. Variation of limit load with edge valency

The limit load based on the value of λ for the configurations with length-to-span ratio of one and uniform gravity load was compared with their average edge valency of vertices and faces (Figure 18). The λ value was maximum for the configuration V.4^4 with the span-to-rise ratio of 6 when the shell structure was supported on the longitudinal edges. For shell structures with all edges supported, configuration V.6^3 with the span-to-rise ratio of 2 was found to have the highest value of λ. For configurations with all edges supported, the limit load increases with the rise-to-span ratio. The additional supports help to increase the load-taking ability of the structure by providing additional load paths.

The value of the parameter λ tends to increase with the edge valency of vertices. Configuration V.4^4 was an exception to this behaviour. This observation clearly states the influence of the orientation of the members (members in adjacent cells) on the overall resistance of the configurations, in addition to the average edge valency. For V.4^4, the transverse members act as an immediate load path and allow easier transfer of the load to the supports (Figure 19). Although the limit load of V.6^3 was higher than that of V.4^4, the weight of V.6^3 was much higher than that of V.4^4. Therefore, the value of λ was higher for the configuration V.4^4. Similar observations were made for these two configurations (V.6^3 and V.4^4) with all the rise-to-span ratios. However, the limit load was lesser for V.4^4

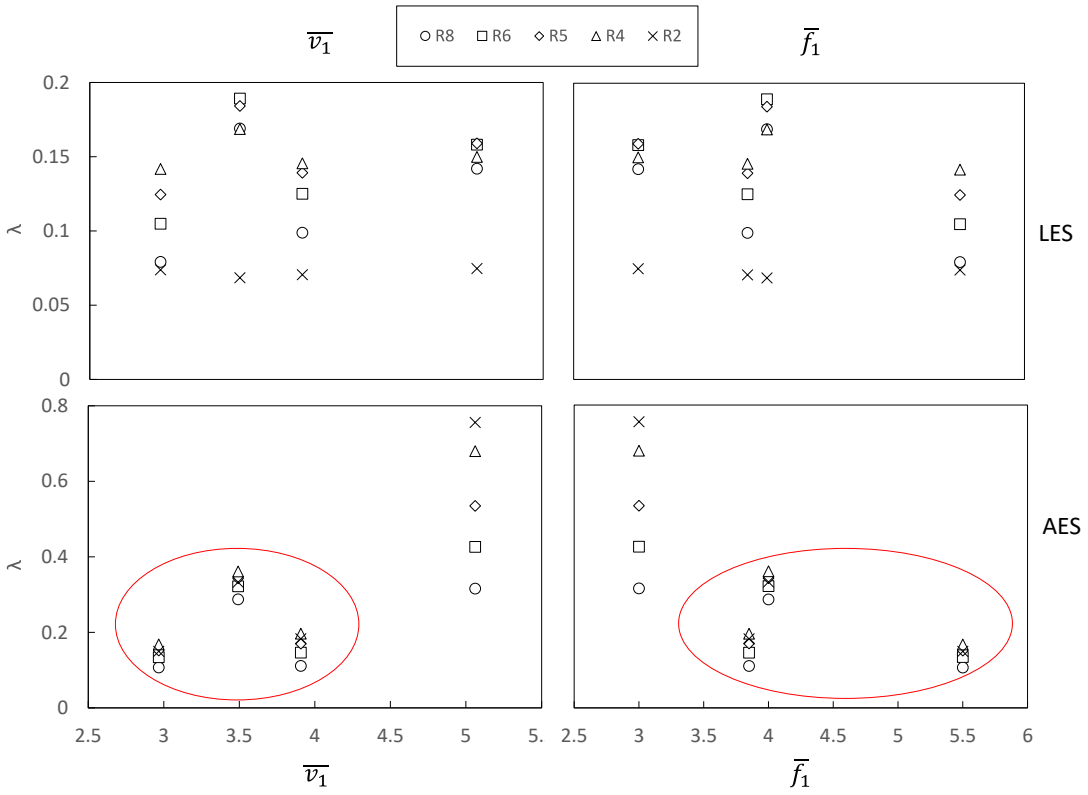

Figure 18: Variation of the parameter λ with average edge valency of vertices and faces for length to span ratio of 1 (L1) and full-span gravity load

with the span-to-rise ratio of two, as the slenderness of the transverse member was very high compared to that of V.6[3], which resulted in a high value of λ for V.6[3] compared to V.4[4] for shell structures with only longitudinal edges were supported. Bracing members play an important role in transferring load to the supports for configurations with all edges supported. Therefore, V.6[3] has better performance compared to the other configurations. The variation of the value of λ is lower with span-to-rise ratio for all the configurations with lower edge valency of vertices (or higher edge valency of faces) and supported on all the edges (AES). In general, load capacity increases with the edge valency of vertices for the selected single-layer reticulated cylindrical shells when all the edges are supported.

The comparison of limit load with the average edge valency of faces shows the exact opposite behaviour to the comparison of limit load with the average edge valency of vertices (Figure 18). The increase in the edge valency of vertices results in the reduction in

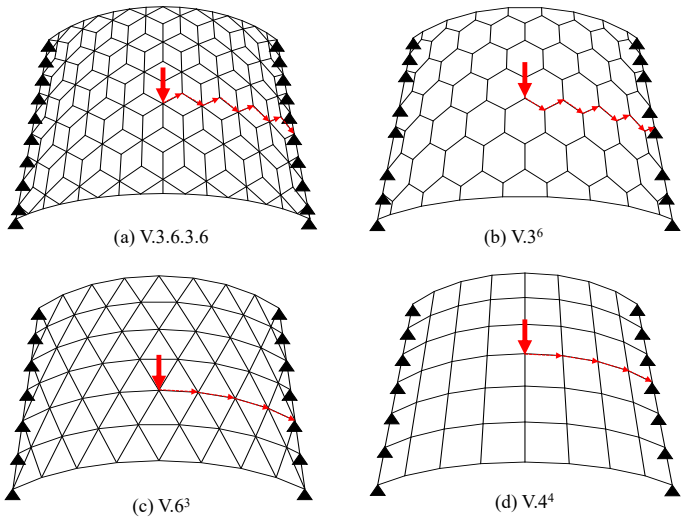

Figure 19: Transfer of load to the support for the shell structures supported only on longitudinal edges

edge valency of faces in any configuration. As a result, the overall resistance of the shell structures increases with a decrease in the edge valency of faces. Equation 39 gives a similar relation between the average edge valency of vertices and the average edge valency of faces when the number of edges in a structure is kept constant

A similar behaviour was observed when the length-to-span ratio of the shell structures was higher. For the length-to-span ratio of 2 (L2), the results are shown in Figure 20.The variation of λ is lower with the span-to-rise ratio for shell structures with lower edge valency of the vertices and supported along all edges. The performance of configuration $V.6^3$ was improved when the length-to-span ratio was higher. $V.4^4$ does not exhibit any advantage when all edges are supported due to the lower advantage provided by the longitudinal members in shell structures with higher length-to-span ratios compared to shell structures with lower length-to-span ratios. Hence, the importance of higher edge valency of vertices (or lower edge valency of faces) is significant when the length of the cylindrical shell structure is much higher compared to the span.

The variation between the load capacity becomes limited once the length-to-span ratio of shell structures becomes higher. There was not much variation in the limit load capacity for L4 structures compared to that of L2 (Figure 21) for all shell structures with longitudinal edge supported (LES). The behaviour of shell structures with both support conditions (LES and AES) was similar when the length-to-span ratio was higher. The curved edge of the shell structure with a large length-to-span ratio, with only longitudinal edges supported, was weak due to the lower edge valency of the edges (Figure 22).

In the next stage, the behaviour of shell configurations with different edge valencies

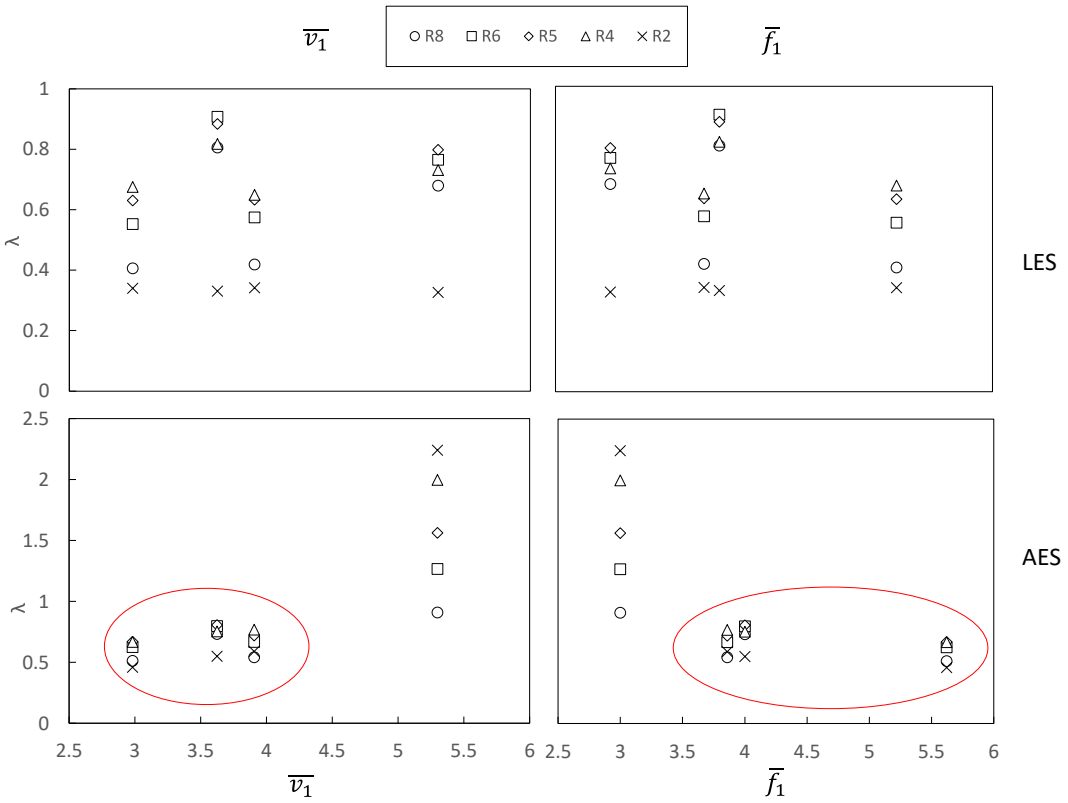

Figure 20: Variation of the parameter λ with average edge valency of vertices and faces for shell structures with length-to-span ratio of 2 (L2) and full-span gravity load application

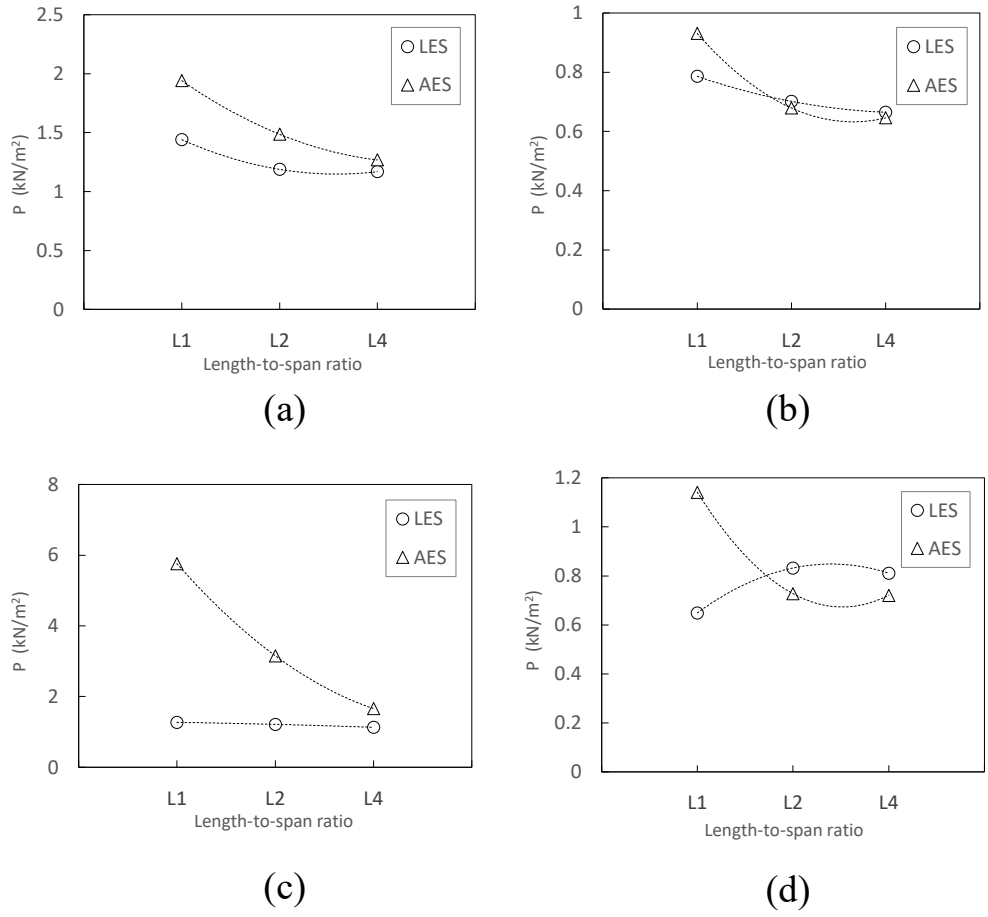

Figure 21: Variation of limit load with change in magnitude of length-to-span ratio (R4-FL): (a) V.3.6.3.6 (b) V.3^6 (c) V.6^3 (d) V.4^4

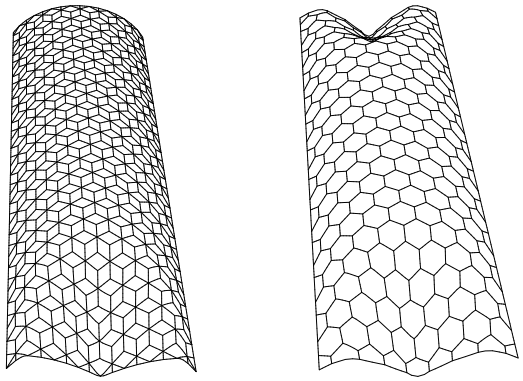

(a) (b)

Figure 22: Failure of shell structures with higher length-to-span ratio (R4-FL): (a) V.3.6.3.6 (b) V.3^6. Failure occurred in regions where lower edge valency of vertices are present.

was studied by subjecting them to semi-span gravity load. The study of unsymmetrical load is important in regions with heavy snowfall. Therefore, investigating the effect of unsymmetrical load on shell configurations will help designers identify which configuration will be highly affected by the unsymmetrical load distribution. The procedure and the parameters adopted were similar to those used in the study of shell structures considering full-span gravity load. The results are provided in Figure 23. The value of λ decreases with the increase in the edge valency of vertices when longitudinal edges are supported. Although the limit load capacity was higher for configurations with a higher average edge valency, the weight of the structures is higher, so the value of λ becomes lower. For shell structures with all edges supported, the value of λ increases with increasing edge valency of the vertices. The results for V.4^4 were different from the observed trend due to the advantage of continuous transverse members available. The behaviour of shell configurations considering average edge valency of the face was precisely opposite to the behaviour of shell structures considering edge valency of vertices.

3.2.3. Limit load of shell structures with initial geometric imperfection

The real world structures will have imperfections and one needs to study the effect of imperfection on shell structures. Hence, the shell structures were subjected to Geometrical and Material Nonlinear Imperfection Analysis (GMNIA) [22] to study the effect of the edge valency on the limit load capacity of the shell structures with initial geometric imperfections. The initial geometric imperfections were provided according to the eigenvalue

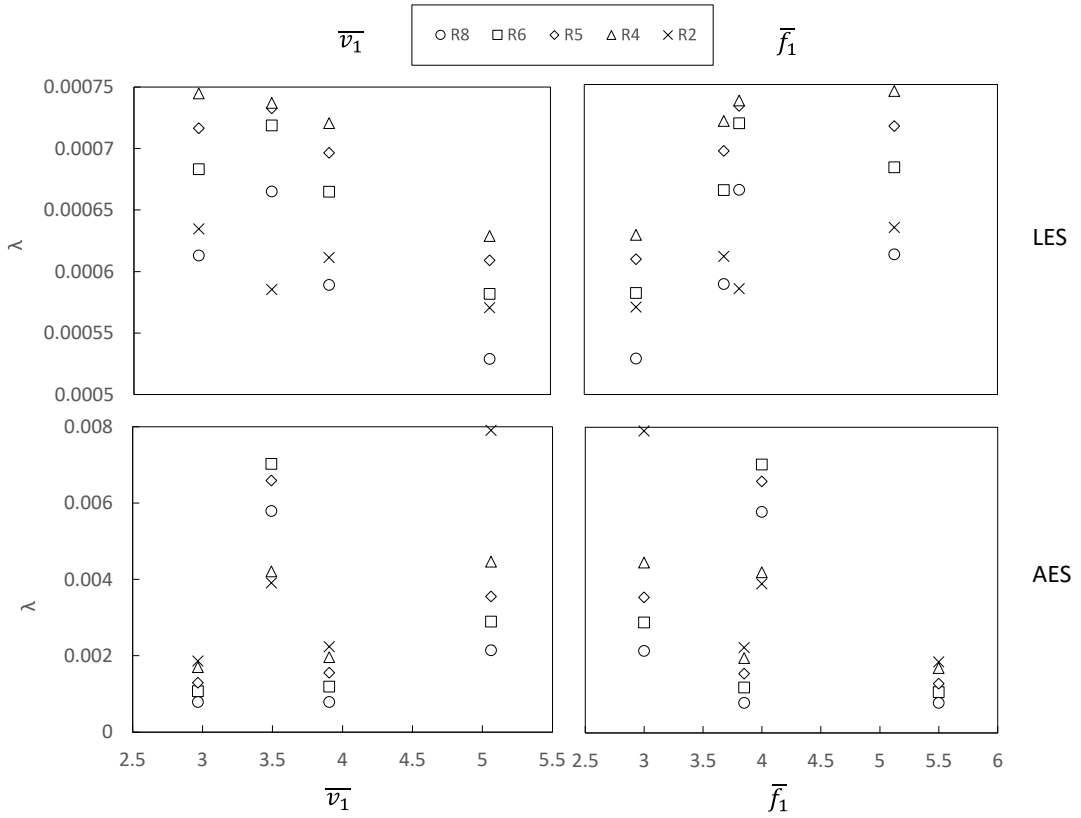

Figure 23: Variation of the parameter λ with average edge valency of the vertices and faces for shell structures subjected to semi-span gravity load and the length-to-span ratio of 1 (L1)

buckling mode method [13]. The imperfections were scaled according to the first buckling mode in the eigenvalue buckling mode method (Figure 16 and Figure 17). The first buckling mode is the most critical mode in most structures, and imperfections modelled as per the first buckling mode provide the structure with the least favourable imperfections.

The different magnitudes of imperfections were considered for the shell structures based on the previous studied conducted (i = S/1000, i = S/500, and i = S/100). Shell structures with longitudinal edge support are more sensitive to initial geometric imperfections than the shell structures with all edges supported (Figure 24 and Figure 25). When the magnitude of the imperfections increases, the effect of edge valency is higher on the limit load capacity for shell structures with longitudinal edges supports (Figure 26). In fact, there is a slight decrease in the value of λ with the increase in the edge valency for configurations with initial geometric imperfections. For configurations with all edges supported, the limit load increases with an increase in the average edge valency of vertices. The reduction in the load capacity with an increase in the initial geometric imperfection is higher for the $V.6^3$ configuration when all the edges were supported. Therefore, the configurations with higher edge valency of the vertices were more affected by the initial geometric imperfections compared to the configurations with lower edge valency. As observed earlier, the effect of the edge valency of faces is exactly opposite to that of the edge valency of vertices (Figure 27), which is in agreement with Equation 39. The parameter λ increases with an increase in the edge valency of faces for shell structures with initial geometric imperfections and longitudinal edges are supported. For configurations with all the edges supported, the parameter λ decreases in general when the average edge valency of the faces increases. Hence, adequate care should be taken while designing structures with a higher edge valency of vertices, as they are more sensitive to initial geometric imperfections and the reduction in load capacity is much higher with increasing geometric imperfection.

In general, an increase in the edge valence of the vertices resulted in an increase in the overall resistance of the shell structures when the connections were rigid. These results were prominent when the shells were supported at all edges, the span-to-rise ratios were within the normal range (0.5-0.8), and the length-to-span ratio was higher (more than one). The results obtained for configuration $V.4^4$ with longitudinal edges supported were slightly different from the noted behaviour due to the importance of transverse members in load transfer to the supports. It is worth considering the orientation of the members, in addition to the edge valency of the members, in fully rigid jointed single-layer reticulated structures.

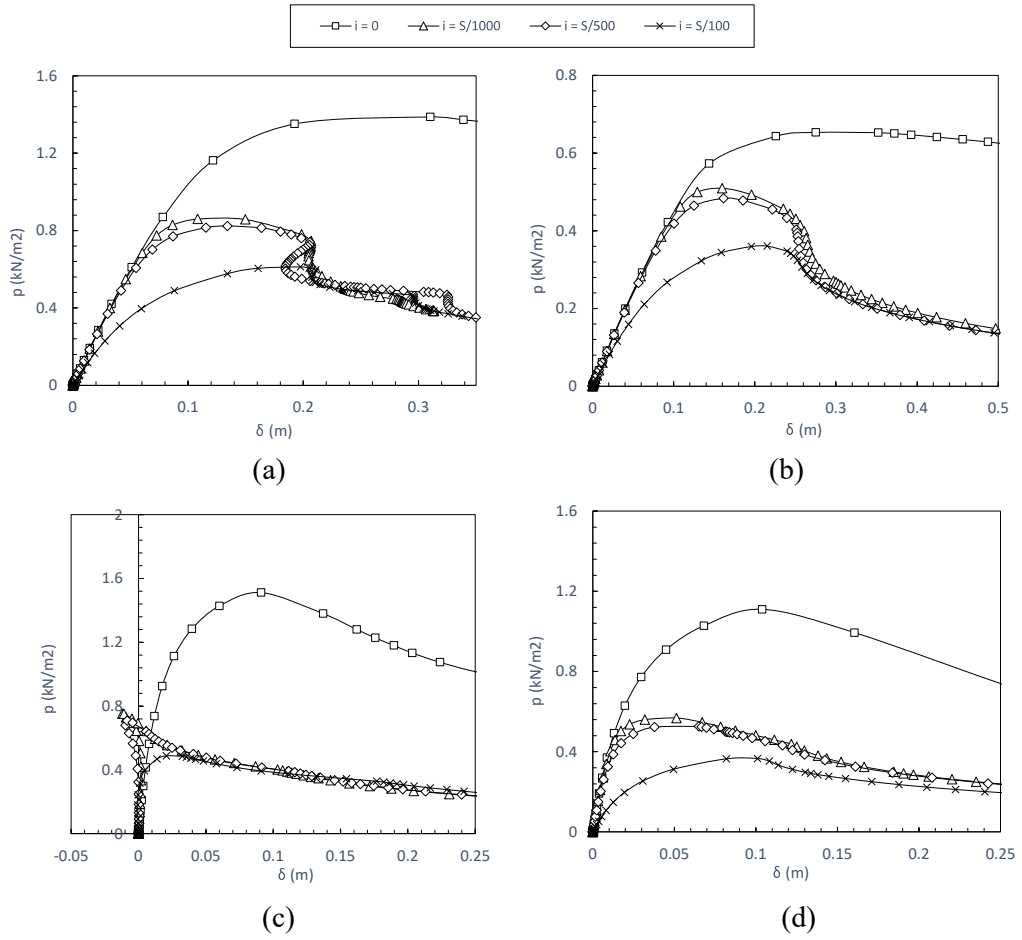

Figure 24: Load-deflection response for shell structures with different magnitude of initial geometric imperfections and longitudinal edge support (L1-R6-FL-LES): (a) V.3.6.3.6 (b) V.3^6 (c) V.6^3 (d) V.4^4

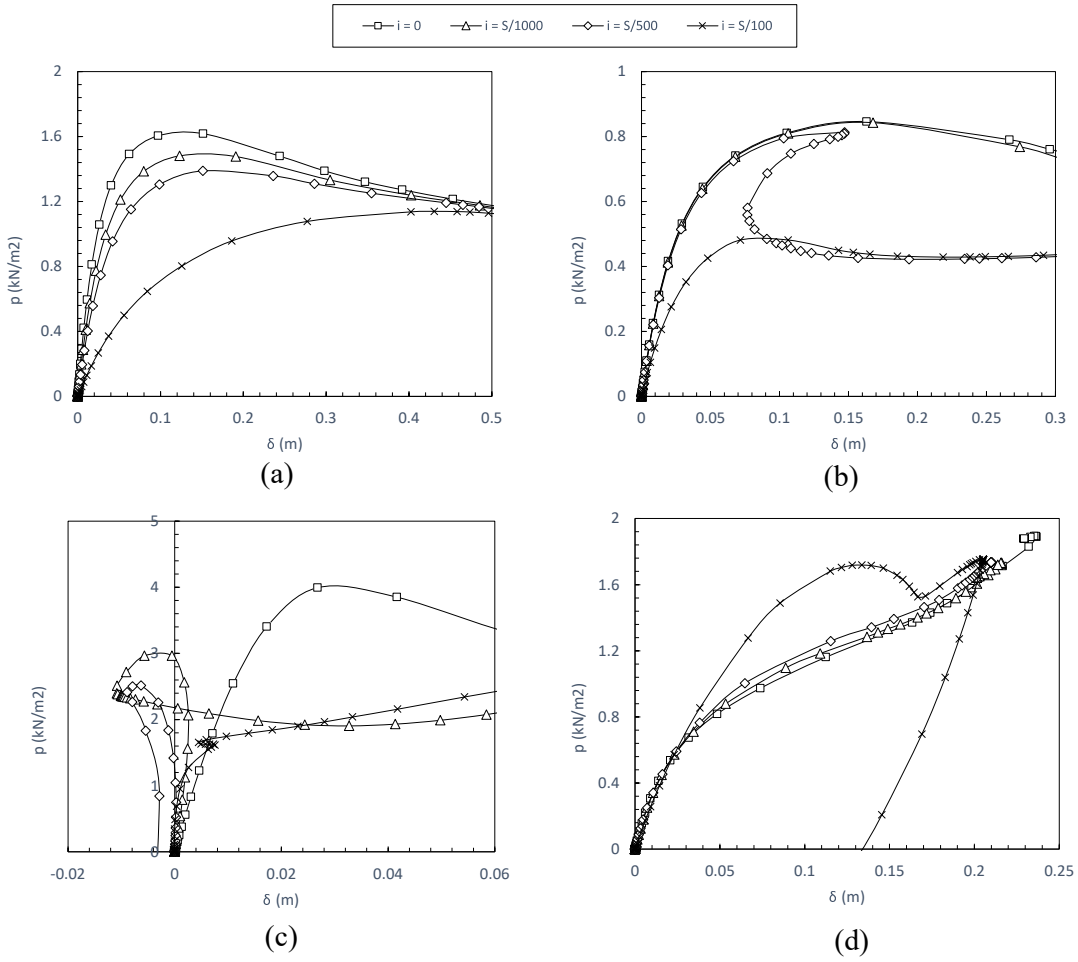

Figure 25: Load-deflection response for shell structures with different magnitude of initial geometric imperfections and supported on all the edges (L1-R6-FL-AES): (a) V.3.6.3.6 (b) V.3^6 (c) V.6^3 (d) V.4^4

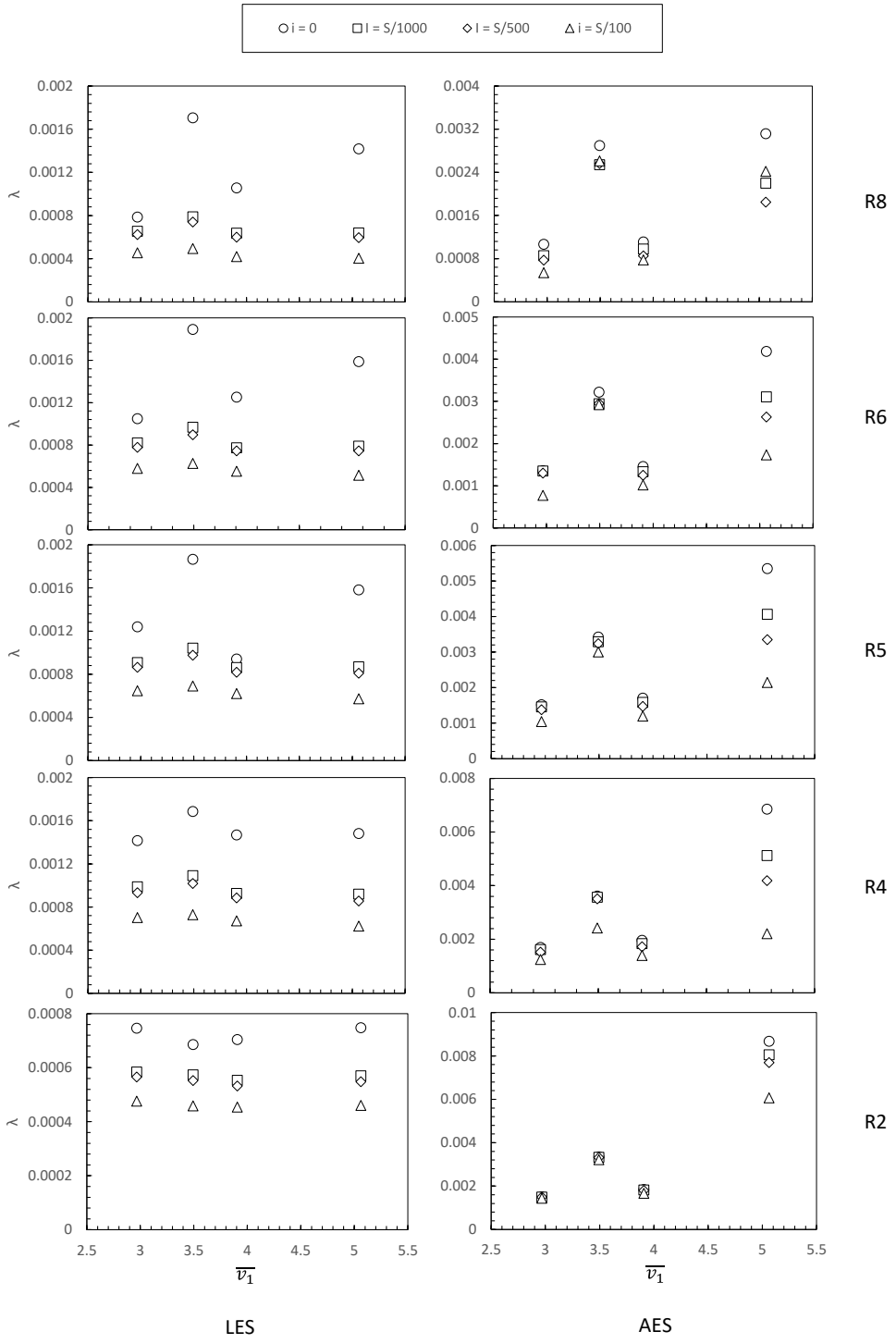

Figure 26: Variation of the parameter λ with average edge valency of the vertices for cylindrical shells with different magnitude of initial geometric imperfection and length to span ratio of 1 (L1)

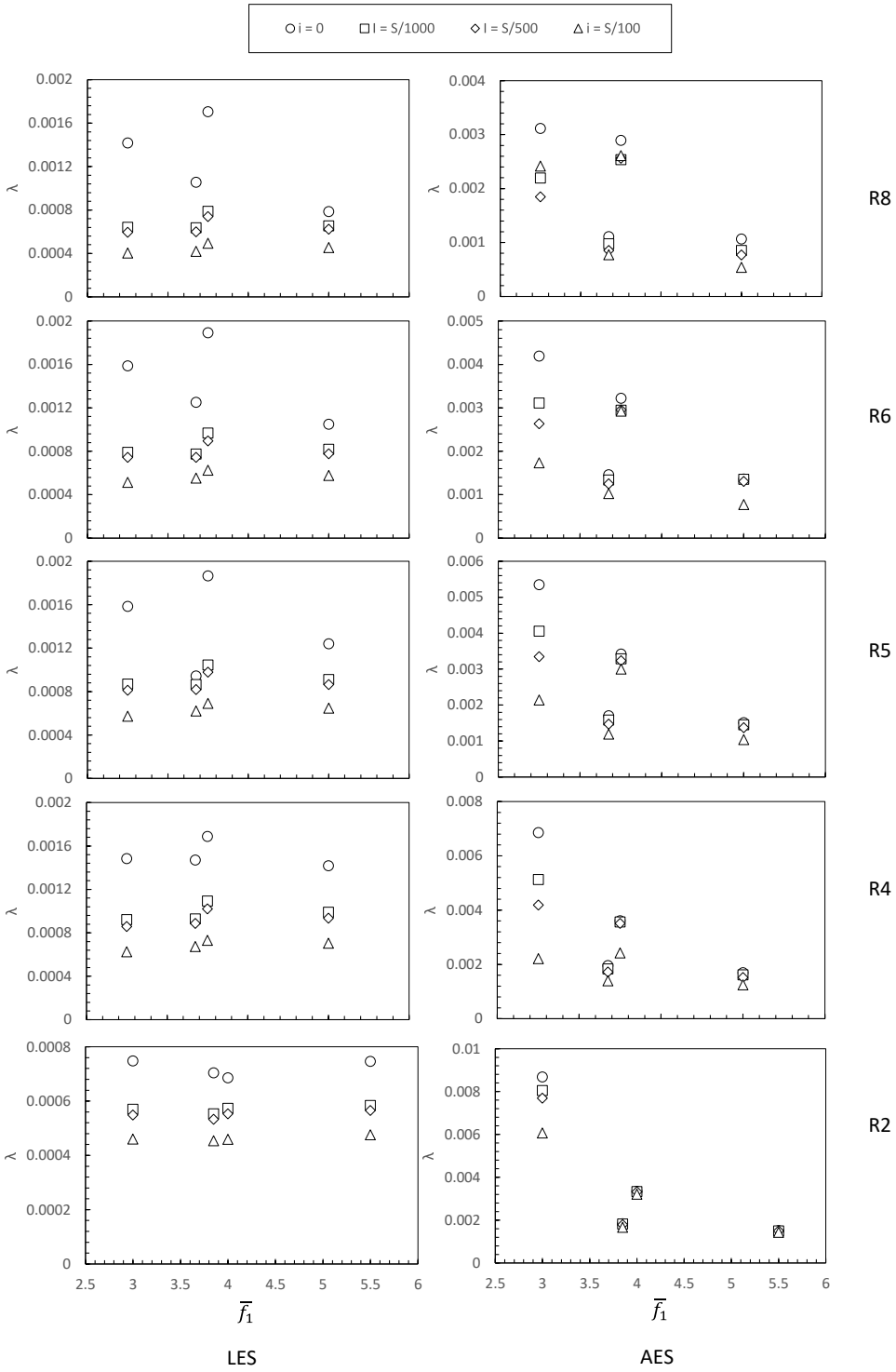

Figure 27: Variation of the parameter λ with average edge valency of the faces for cylindrical shells with different magnitude of initial geometric imperfection and length to span ratio of 1 (L1)

4. Discussion

One of the main goals of this study was to predict the effect of edge valency of the vertices and faces on the limit load capacity of the single-layer reticulated cylindrical shells. The nonlinear analysis revealed that the overall resistance of the reticulated shells improves with increasing edge valency of vertices and decreasing edge valency of the faces for most of the configurations. In addition to that, the support conditions, the rise-to-span ratio, and the load pattern influence how the limit load varies with the edge valency. The influence of the edge valency was more substantial for the shell structures when all edges were supported (such as indoor stadiums and exhibition halls) than when only the longitudinal edges were supported (such as railway station platforms). For structures supported by longitudinal edges, transverse members play a more prominent role in addition to edge valency in overall stability [16]. The present study reinstates the importance of transverse members in the load path for shell structures supported on longitudinal edges. Configuration V.4^4 has a higher 'limit load/weight' value compared to V.6^3. Although the load-bearing capacity of the V.6^3 configuration was higher, the weight of the members was so large compared to the V.4^4 configuration, resulting in a lower limit load to weight ratio. Hence, V.4^4 configuration with rigid connections between the members can be safely adopted for shell structures with lower spans and lower load requirements. The consideration of edge valency of the shell configuration alone is not adequate for predicting the performance of the shell configuration, and the orientation of the members should be considered by introducing the angle between the members in the adjacent faces. Analysis of configurations with a higher length-to-span ratio, semi-span gravity load, and initial geometric imperfections indicates a similar result.

All the results indicate that the higher edge valency of faces will reduce the limit load, as higher edge valency of faces reduces the edge valency of vertex in a configuration. Hence, the influence of edge valency of vertices alone can determine the behaviour of the shell configurations to a great extent. Again, the orientation of the members, member slenderness, rise-to-span ratio, and support condition play a crucial role in the behaviour of shell structures in addition to the edge valency.

As stated earlier, optimising all the elements in a structure is difficult to achieve. Optimising one element will lead to a disproportionate variation in the value of other elements (Table 3). Hence, a multi-dimensional optimisation technique is required to study the effect of a single parameter, keeping others as equal as possible across all the configurations. The present investigation monitored a limited number of samples, while a larger number of samples could clearly indicate how edge valency will affect the overall stability of single-layer reticulated structures.

The large-span single-layer domes cannot be tested in their actual dimensions, and the scaled prototypes will not provide the actual behaviour of the reticulated shells due to their

size effect. The experimental study of a substructure with actual dimensions of the members and connections is possible when the actual stiffness of the boundaries is modelled. Identifying the average valency in a shell structure will indirectly provide the influence of joint stiffness on the resistance of single-layer reticulated shells with rigid jointed members. Testing the substructures of the actual shell configurations is possible the relative rigidity of the boundary of the considered shell substructure is known, by calculating with the help of the average edge valency of elements. Hence, investigating the average value of edge valency will help to calculate the relative stiffness of the boundaries to be adopted for the substructure. A greater understanding of the present findings could also lead to the theoretical improvement in how a configuration can be modified such that triangulation may not be required for structures where joints are rigid, and load requirements are limited; thereby reducing the total cost of the structure.

5. Concluding Remarks

The influence of the edge valency of the vertices and faces on the overall resistance of single-layer reticulated cylindrical shells was studied, considering four configurations. The results show that the limit load capacity increases with the edge valency of vertices and decreases with the edge valency of faces. An increase in the edge valency of vertices in a shell structure results in a reduction of the average edge valency of faces; hence, one parameter is sufficient to study the relation of edge valency with the overall stability of single-layer reticulated cylindrical shells. The optimum rise-to-span ratio corresponds to the maximum 'strength-to-weight' ratio changes with the type of configuration and the support condition. In fact, the support condition defines which configuration is optimum based on the available load paths. When all the edges are supported – such as the roof of an indoor stadium with four walls around – the edge valency of vertices plays a crucial role in governing the overall resistance of the shell structure. Triangulated shell configurations provide the maximum edge valency of vertices (i.e., minimum edge valency of faces), thereby resulting in the most stable single-layer cylindrical shell configuration among the shell structures considered. However, configurations such as V.4^4 with rigidly connected members can be adopted when the span and load requirement are lower, as the strength-to-weight ratio is higher for V.4^4 compared to V.6^3. Therefore, the present study reveals the effect of edge valency on the overall resistance of single-layer reticulated shell structures. The data on the edge valency helps the designer optimise the structure so that the resistance is not compromised.

Although only four configurations with limited parameters are investigated in this study, multi-parameter optimisation techniques will reinstate the importance of the edge valency in the single-layer reticulated shell configurations. The same concept can be extended to multi-layer reticulated shell structures, as the concept is valid for any structure

in three-dimension. Hence, future work will mainly cover the influence of edge valency in double-layer reticulated shell structures and the involvement of member orientation in global and local stability.

References

[1] N. Subramanian, Principles of space structures, Wheeler, 1999.

[2] G. Ramaswamy, M. Eekhout, Analysis, design and construction of steel space frames, Thomas Telford, 2002.

[3] Z. Makowski, History and development of various types of braced barrel vaults and review of recent achievements all over the world, in: Z. Makowski (Ed.), Analysis, design, and construction of braced barrel vaults, Granada Publishing Ltd., 1985.

[4] G. Parke, Comparison of the structural behaviour of various types of braced barrel vaults, in: Z. Makowski (Ed.), Analysis, design, and construction of braced barrel vaults, Routledge, 1985, pp. 90 – 120.

[5] V. Gioncu, Buckling of reticulated shells: state-of-the-art, International Journal of Space Structures 10 (1) (1995) 1–46. doi:10.1177/026635119501000101.

[6] K. Abedi, Propagation of local instabilities in braced domes, Ph.D. thesis, University of Surrey (1997).

[7] P. Lenza, Instability of single layer doubly curved vaults, International Journal of Space Structures 7 (4) (1992) 253–264. doi:10.1177/026635119200700403.

[8] S. Kato, T. Yamashita, Evaluation of buckling load of two-way single layer grid shells, Journal of the International Association for Shell and Spatial Structures 51 (2) (2010) 109–123.

[9] S. Yamada, A. Takeuchi, Y. Tada, K. Tsutsumi, Imperfection-sensitive overall buckling of single-layer lattice domes, Journal of engineering mechanics 127 (4) (2001) 382–386. doi:10.1061/(ASCE)0733-9399(2001)127:4(382).

[10] A. López, I. Puente, M. A. Serna, Numerical model and experimental tests on single-layer latticed domes with semi-rigid joints, Computers & structures 85 (7-8) (2007) 360–374. doi:10.1016/j.compstruc.2006.11.025.

[11] F. Fan, Z. Cao, S. Shen, Elasto-plastic stability of single-layer reticulated shells, Thin-Walled Structures 48 (10-11) (2010) 827–836. doi:10.1016/j.tws.2010.04.004.

[12] J. Yan, F. Qin, Z. Cao, F. Fan, Y. Mo, Mechanism of coupled instability of single-layer reticulated domes, Engineering Structures 114 (2016) 158–170. doi:10.1016/j.engstruct.2016.02.005.

[13] X. Chen, S.-Z. Shen, Complete load-deflection response and initial imperfection analysis of single-layer lattice dome, International Journal of Space Structures 8 (4) (1993) 271–278. doi:10.1177/026635119300800405.

[14] F. Fan, J. Yan, Z. Cao, Elasto-plastic stability of single-layer reticulated domes with initial curvature of members, Thin-Walled Structures 60 (2012) 239–246. doi:10.1016/j.tws.2012.01.012.

[15] F. Liu, R. Feng, K. D. Tsavdaridis, G. Yan, Designing efficient grid structures considering structural imperfection sensitivity, Engineering Structures 204 (2020) 109910. doi:10.1016/j.engstruct.2019.109910.

[16] A. El-Sheikh, Configurations of single-layer barrel vaults, Advances in Structural Engineering 4 (2) (2001) 53–64. doi:10.1260/1369433011502354.

[17] A. El-Sheikh, Performance of single-layer barrel vaults with different configurations, International Journal of Space Structures 16 (2) (2001) 111–123. doi:10.1260/0266351011495214.

[18] A. El-Sheikh, Effect of geometric imperfections on single-layer barrel vaults, International Journal of space structures 17 (4) (2002) 271–283. doi:10.1260/026635102321049538.

[19] M. Mohammadi, K. Abedi, N. Taghizadieh, Stability analysis of single-layer barrel vault space structures, International Journal of Space Structures 27 (4) (2012) 203–218. doi:10.1260/0266-3511.27.4.203.

[20] A. Loeb, Space structures, Springer Science & Business Media, 2012.

[21] R. Kolakkattil, A. Jayachandran, Global stability behaviour of single-layer reticulated domes created using a new nomenclature, Journal of the International Association for Shell and Spatial Structures 63 (1) (2022) 31–48. doi:10.20898/j.iass.2021.012.

[22] European Committee for Standardization (CEN), Eurocode 3: Design of steel structures–part 1-6: Strength and stability of shell structures (EN 1993-1-6), 2007.

[23] H. Nooshin, P. Disney, Formex configuration processing i, International journal of space structures 15 (1) (2000) 1–52. doi:10.1260/0266351001494955.

[24] ABAQUS Inc., ABAQUS/Standard User's Manual, Version 6.9, Dassault Systems Simulia Corp, Providence, RI, 2009.

[25] Bureau of Indian Standard, IS 1161 – 1998: Steel tubes for structural purposes – specifications, BIS, New Delhi, India, 1998.

[26] Bureau of Indian Standard, IS 800 - 2007: General construction in steel-code of practice, BIS, New Delhi, India, 2007.

[27] D. T. Wright, Membrane forces and buckling in reticulated shells, Journal of the structural division 91 (1) (1965) 173–201. doi:10.1061/JSDEAG.0001205.

Nomenclature

$\bar{c_0}$ Average vertex valency of cells in a structure

$\bar{c_1}$ Average edge valency of cells in a structure

$\bar{c_2}$ Average face valency of cells in a structure

$\bar{e_0}$ Average vertex valency of edges in a structure

$\bar{e_2}$ Average face valency of edges in a structure

$\bar{e_3}$ Average cell valency of edges in a structure

$\bar{f_0}$ Average vertex valency of faces in a structure

$\bar{f_1}$ Average edge valency of faces in a structure

$\bar{f_3}$ Average cell valency of faces in a structure

$\bar{v_1}$ Average edge valency of vertices in a structure

$\bar{v_2}$ Average face valency of vertices in a structure

$\bar{v_3}$ verage cell valency of vertices in a structure

δ Vertical deflection of the apex node of the shell structure (m)

ϵ	Engineering strain
ϵ_y	Yield strain of steel
λ	The limit load capacity per unit weight of the structure
σ	Engineering stress
$B31$	Two noded linear beam element used in Abaqus CAE
C_0	Vertex valency of a cell
C_1	Edge valency of a cell
C_2	Face valency of a cell
E_0	Vertex valency of an edge
E_2	Face valency of an edge
E_3	Cell valency of an edge
F_0	Vertex valency of a face
F_1	Edge valency of a face
F_3	Cell valency of a face
f_y	Yield stress of steel
i	The maximum magnitude of initial geometric imperfection applied to the structure
L	Length of the shell structure
N_i	The number of elements with dimensionality i
N_0	Number of vertices in a structure
N_1	Number of edges in a structure
N_2	Number of faces in a structure
N_3	Number of cells in a structure
N_x^y	Number of elements with dimensionality ‘x’ and valency corresponding to the dimensionality ‘y’

P	Limit load of the shell structure per unit area (kN/m^2)
p	Load applied on the shell structure per unit area (kN/m^2)
R	Rise of the shell structure
S	Span of the shell structure
V_1	Edge valency of a vertex
V_2	Face valency of a vertex
V_3	Cell valency of a vertex
W	Total weight of the structure